



1 Changes in extremely hot days under stabilized 1.5°C and 2.0°C global warming
2 scenarios as simulated by the HAPPI multi-model ensemble

3
4 Michael Wehner^{1*}, Dáithí Stone¹, Dann Mitchell², Hideo Shiogama³, Erich Fischer⁴,
5 Lise S. Graff⁵, Viatcheslav V. Kharin⁶, Ludwig Lierhammer⁷, Benjamin Sanderson⁸,
6 Harinarayan Krishnan¹

7
8 ¹ Lawrence Berkeley National Laboratory, Berkeley, California 94720, USA

9 ² University of Bristol, Bristol, United Kingdom

10 ³ National Institute for Environmental Studies, Tsukuba, Ibaraki 305-8506, Japan

11 ⁴ ETH Zurich, Switzerland

12 ⁵ Norwegian Meteorological Institute, Oslo, Norway

13 ⁶ Canadian Centre for Climate Modelling & Analysis, Victoria, British Columbia,
14 Canada

15 ⁷ German Climate Computing Center (DKRZ) Hamburg, Germany

16 ⁸ National Center for Atmospheric Research, Boulder, Colorado, USA

17 * Corresponding Author: mfwehner@lbl.gov

18

19 **Abstract**

20 The Half A degree additional warming, Prognosis and Projected Impacts (HAPPI)
21 experimental protocol provides a multi-model database to compare the effects of
22 stabilizing anthropogenic global warming of 1.5°C over preindustrial levels to 2.0°C
23 over these levels. The HAPPI experiment is based upon large ensembles of global
24 atmospheric models forced by sea surface temperature and sea ice concentrations
25 plausible for these stabilization levels. This paper examines changes in extremes of
26 high temperatures averaged over three consecutive days. Changes in this measure
27 of extreme temperature are also compared to changes in hot season temperatures.
28 We find that the differences between the two stabilization scenarios in extreme high
29 temperatures over land ranges from about 0.25 to 1.0°C depending on location and
30 model. Results from the HAPPI models are consistent with similar results from the
31 one available fully coupled climate model. However, a complicating factor in
32 interpreting extreme temperature changes across the HAPPI models is their
33 diversity of aerosol forcing changes.

34

35 **Introduction**

36 The United Nations Framework Convention on Climate Change (UNFCCC)
37 challenged the scientific community to describe the impacts of stabilizing the global
38 mean temperature at its 21st Conference of Parties held in Paris in 2016. A specific
39 target of 1.5°C above preindustrial levels had not been seriously considered by the
40 climate modeling community prior to the Paris Agreement. Indeed, this level of
41 global warming is reached but then exceeded in most of the projections of the
42 Coupled Model Intercomparison Project (CMIP5), the source of much of our detailed
43 information about projected future climate change scenarios (Collins et al. 2013).
44 Analysis of these transient global climate model simulations as they pass through
45 1.5 and 2.0°C warmer temperatures than preindustrial estimates are not necessarily
46 descriptive of a stabilized climate due to the differential warming rates over land



47 and ocean regions of the planet. While pattern scaling (Tebaldi and Arblaster 2014)
48 of stabilized simulations at warmer levels may permit reasonable estimate of
49 surface air temperature and precipitation at the Paris Agreement targets, such
50 techniques have not been widely applied to other important output quantities from
51 climate models. Hence, custom simulations tailored to these 1.5 and 2.0°C targets
52 outside of the CMIP5 (and CMIP6) protocols are the most straightforward vehicles
53 for the scientific community to inform the UNFCCC.

54

55 Recently, the modeling group at the National Center for Atmospheric Research
56 (NCAR) performed simulations of the Community Earth System Model (CESM1)
57 suitably forced to stabilize to the Paris Agreement targets. Described in Sanderson
58 et al. (2017), these ocean-atmosphere coupled global simulations extend a previous
59 large ensemble (Kay et al. 2015) and provide a rather complete description of the
60 climate system at these stabilized levels and a path toward stabilization. However,
61 to more fully understand the model structural uncertainty in such projections,
62 efforts from additional modeling groups are necessary. In lieu of an internationally
63 coordinated extension to CMIP6 and to provide information prior to the publication
64 deadlines to the special report requested of the Intergovernmental Panel on Climate
65 Change, a limited number of modeling groups agreed to a simpler set of customized
66 simulations. The HAPPI experiment (Half A degree additional warming, Prognosis
67 and Projected Impacts) is based on the atmospheric components of CMIP5 models
68 forced by prescribed sea surface temperature (SST) and sea ice concentrations
69 (Mitchell et al. 2017). By replacing the ocean and sea ice components models with
70 prescribed values, simulation workflows are considerably simplified and
71 computational resource requirements reduced enabling the integration of larger
72 ensembles. SST and associated sea ice concentrations were specially constructed for
73 the HAPPI experimental protocol. SSTs for the 1.5°C stabilization scenario are scaled
74 from the CMIP5 RCP2.6 simulations and a combination of the RCP2.6 and RCP4.5
75 simulations for the 2°C stabilization scenario. Sea ice concentrations are computed
76 using an adapted version of the method described in Massey (2017) by using
77 observations of SST and ice to establish a linear relationship between the two fields
78 for the time period 1996-2015 and are consistent with the HAPPI prescribed SST
79 fields. Details are further described in Mitchell et al. (2017). While HAPPI allows for
80 large ensembles of multiple models to be compared, there are tradeoffs to note in
81 this simpler approach to modeling a stabilized climate including the potential for
82 radiative imbalance and inconsistencies between the atmospheric state and the
83 surface at the sea ice/ocean boundaries (Covey et al. 2004). Furthermore, while
84 CMIP5 model differences in equilibrium climate sensitivity are largely due to
85 differences in ocean heat uptake (Collins et al. 2013), important residual differences
86 remain over land and global mean temperatures that are not the same across the
87 participating models. Finally, due to the prescribed SSTs HAPPI does not account for
88 different realizations of or potential changes in ocean internal variability. The
89 present study is confined to changes in extreme temperatures over land simulated
90 for the HAPPI project and defers these issues to later analyses.

91

92 **Data and Methods**



93 Five modeling groups have submitted model output data to the HAPPI project that is
94 freely available to the public. Model #1 is the NCAR-DOE Community Atmosphere
95 Model version 4 (CAM4) coupled to the Community Land Model version 4 (CLM4)
96 with simulations contributed by ETH Zurich (Neale et al. 2011; Oleson et al. 2010).
97 Model #2 is the Canadian Fourth Generation Atmospheric Global Climate Model
98 (CanAM4) contributed by the Canadian Centre for Climate Modelling and Analysis
99 (von Salzen et al. 2013). Model #3 is ECHAM6.3 (Stevens et al. 2013), contributed by
100 the Max Planck Institute for Meteorology, Hamburg, Germany. It includes a modified
101 version of the land component (Reick et al. 2013). The soil hydrology is described by
102 a 5-layer scheme (Hagemann and Stacke 2015) instead of the bucket scheme used in
103 the CMIP5 version. Additionally, a high resolution (global 0.5° grid) hydrological
104 discharge model (Hagemann and Dümenil, 1997) is activated. Model #4 is the
105 MIROC5 model contributed by the National Institute for Environmental Studies,
106 Tsukuba, Japan and denoted as “MIROC5” (Shiogama et al. 2013, 2014). Model #5
107 (NorESM1) is an updated version of the Norwegian Earth System model version 1
108 (Bentsen et al. 2013, Iversen et al. 2013), contributed by the Norwegian Climate
109 Center. The NorESM1 is based on the NCAR Community Climate System Model
110 version 4 (Gent et al., 2011), but with a different ocean model and a modified
111 atmosphere component. The atmosphere model is based on the Community
112 Atmosphere Model version 4, but includes an advanced module for aerosols and
113 aerosol-cloud-radiation interactions (Kirkevåg et al. 2013). The version of the
114 NorESM1 used in the HAPPI project, NorESM1-Happi, additionally includes
115 improvements to wet snow albedo, and the atmospheric burden of soot (Iversen et
116 al, in prep.).

117
118 Aerosol forcings are not prescribed but left to the modeling groups to implement
119 based on their previous experience and simulations. The only constraint specified
120 by the HAPPI protocol is that the 1.5°C and 2°C use the same aerosol forcing.
121 Variations between model treatments in both the absolute magnitudes of the
122 aerosol forcing as well as their differences in the historical and stabilized scenarios
123 will prove to be an important factor in the changes in extreme temperatures.

124
125 An additional model result is also presented for comparison. The Community Earth
126 System Model (CESM1) is a fully coupled model that was not part of the HAPPI
127 project. However, 15 member ensembles of simulations were made under forcing
128 scenarios tailored to produce 1.5°C and 2°C stabilized climates (Sanderson et al.
129 2017). These simulations, while not directly comparable to the five HAPPI models,
130 provide additional context for extreme temperatures in stabilized low warming
131 scenarios.

132
133 The HAPPI experimental protocol was inspired by the “Climate of the 20th Century
134 Plus (C20C+) Detection and Attribution project” (Stone et al. 2017) and data from
135 both sets of simulations are available at the same website (portal.nersc.gov/c20c).
136 However, only output from the MIROC5 model was submitted to both projects. In
137 the HAPPI experimental protocol, the present day forcings and boundary conditions
138 are representative of the observed 2006-2015 state and is identical to that specified



139 in the C20C+ protocol over that period. HAPPI forcings for stabilized future
140 scenarios preserve the observed 2006-2015 interannual variability (Stone et al.
141 2017; Mitchell et al. 2017) but include appropriate changes derived from the CMIP5
142 RCP2.6 and RCP4.5 scenario simulations. Dates for these simulations are nominally
143 2106-2115 as atmospheric trace gas concentrations are scaled from the RCP's
144 protocol at 2095. The C20C+ protocol also includes a similar non-industrial
145 representation of the climate with anthropogenic changes removed from the
146 observed SST and sea ice concentrations (Stone et al. 2017). Table 1 summarizes
147 details of the model simulations used in this study. Note that the ensemble sizes are
148 exceptionally large for a publicly available multi-model climate simulation dataset.
149

150 In this study, we examine the differences in changes in extreme temperatures from
151 the HAPPI simulations. In a companion paper, we examined such changes between
152 the actual and counterfactual (non-industrialized) simulations submitted to the
153 C20C+ project and this paper uses the same extreme value statistical methodologies
154 (Wehner et al. 2017). The annual maximum of the daily maximum temperature is
155 one of the 27 indices defined by the Expert Team on Climate Change Detection
156 Indices (ETCCDI) and is a robust indicator of extremely hot weather (Zhang et al.
157 2011). Called "TXx" by the ETCCDI and derived from "tasmax", the daily maximum
158 near surface air temperature in the CMIP5, this quantity is also known as "hot days"
159 because it is the hottest daytime temperature of the year. As in our previous work
160 on this topic (Tebaldi and Wehner 2016; Sanderson et al. 2017; Wehner et al. 2017),
161 we first calculate the running 3 day average of tasmax and compute its annual
162 maximum, denoted hereafter as TX3x, and then estimate its 20 year return values
163 using a block maxima technique. We have previously found that while long period
164 return values of TX3x are slightly smaller than for the daily quantity, projected
165 changes of the 3 day averages were considerably larger. For this study, where we
166 are interested in the small differences between the 1.5°C and 2.0°C stabilization
167 levels, this point becomes particularly important.
168

169 In this paper, we do not assess the HAPPI models' relative skill at reproducing
170 observed estimates of extremes temperatures. However, we note that this set of
171 models form the atmospheric components of several of the CMIP5 fully coupled
172 models. Sillman et al. (2014) did examine the CMIP5 model's performance in
173 simulating TXx and other ETCCDI measures. The coupled models corresponding to
174 these five HAPPI models spanned a large range of TXx errors when compared to
175 four different reanalyses. These model errors are presumably reduced when the
176 ocean is specified to its observed state.
177

178 As in our C20C+ analysis of anthropogenic extreme temperature changes, we
179 estimate 20-year return values by fitting the Generalized Extreme Value (GEV)
180 distribution by the methods of L-moments (Hosking and Wallis 1997). Assumptions
181 that the analyzed data is stationary and independent and identically distributed
182 (i.i.d) are necessary for this approach to be valid and are reasonable for the HAPPI
183 model output. A more detailed discussion of the rationale and limitations of these
184 assumptions for the C20C+ data is provided in Wehner et al. (2017) and the same



185 arguments hold for the HAPPI data. The large ensemble sizes of the HAPPI models
186 (table 1) ensure that uncertainty due to the fitting of statistical distribution is
187 negligible.

188

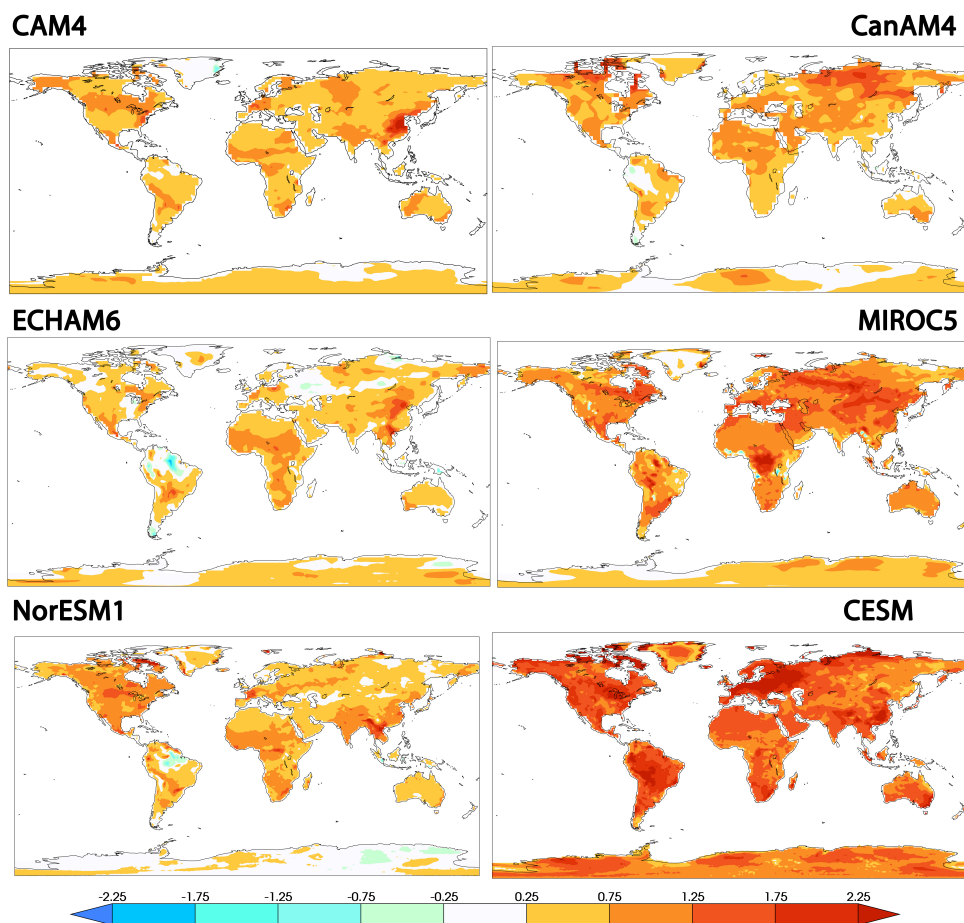
189 **Results**

190 In Wehner et al. (2017), we showed that changes in extreme temperatures at a fixed
191 rarity are insensitive to the specification of that rarity (i.e. the length of the return
192 period) due to the bounded nature of fitted GEV distributions. Conversely, we
193 further showed as a consequence of the shape of bounded GEV distributions, that
194 changes in the probabilities of extreme temperatures of fixed magnitudes are
195 sensitive to small differences in that specified magnitude. Both ways of expressing
196 changes in extreme temperatures can be useful. This first method would be useful if
197 a system (for instance, a cooling system for a computer center or factory) must be
198 designed to operate with a specified mean time to failure by informing how the
199 critical temperature would change. On the other hand, health advisories are often
200 issued when temperatures exceed a critical value and the second method would
201 inform how frequent such advisories would be issued in a warmer world.

202

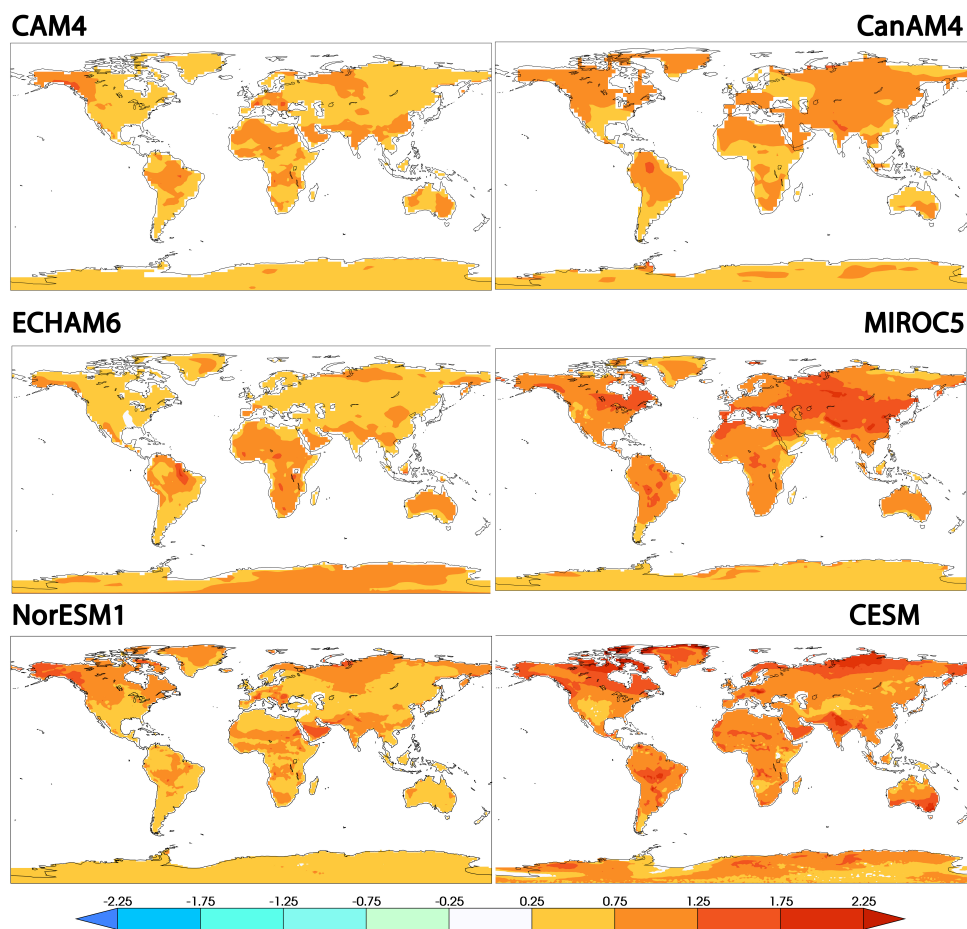
203 We limit this study to this first method by reporting changes in 20 year return
204 values of extreme temperatures with the recognition that changes in longer period
205 return values do not differ greatly. This is principally due to the bounded nature of
206 the fitted GEV distributions and little difference in the width of these distributions
207 over most land areas (Wehner et al. 2017). As changes in return periods for fixed
208 thresholds are not as stable to the choice of threshold values, any results we might
209 report would be of less general utility so we defer such to more targeted impact
210 analyses. Figure 1 shows the changes over land in 20 year return values of the
211 annual maximum of the three day average of daily maximum surface air
212 temperatures ($TX3x$) between the 1.5°C stabilized scenario and the present day
213 simulations. Of the HAPPI models, MIROC5 exhibits the largest increases of the five
214 HAPPI models exceeding 0.75°C nearly everywhere and even 1.25°C over large
215 regions. CAM4 and ECHAM6 exhibit the smallest changes but do have hot spots in
216 Asia. CanAM4, ECHAM6 and NorESM1 also show decreases or little increase over
217 parts of the Amazon, but MIROC5 does not. The fitted GEV parameters and hence
218 these return value changes are extremely robust to sample size uncertainty due to
219 the large number of realizations in the HAPPI database (Table 1). Standard errors
220 determined by a bootstrap calculation (Hoskins and Wallis 1997) are very small.

221



222
223 Figure 1. Change in 20 year return values (°C) between the 1.5°C and present day
224 HAPPI simulations of TX_{3x} . Upper left: CAM4. Upper right: CanAM4. Middle left:
225 ECHAM6. Middle right: MIROC5. Lower left: NorESM1. Lower right: CESM.
226

227 The annual maximum of the daily high temperature is most likely to occur in the
228 summer over most of the world outside of the tropics. Figure 2 shows the difference
229 between the 1.5°C stabilized scenario and the present day simulations of the
230 average surface air temperature in the hottest season, usually June-July-August in
231 the Northern Hemisphere and December-January-February in the Southern
232 Hemisphere. This much more spatially smooth average temperature change is quite
233 different from the extreme temperature change in other ways as well. Global land
234 average differences (shown in table 1) indicate that hot season temperatures
235 generally increase slightly more than extreme temperatures. Furthermore, there are
236 no regions of average temperature decreases. Average temperature increases are
237 always greater than 0.25°C.

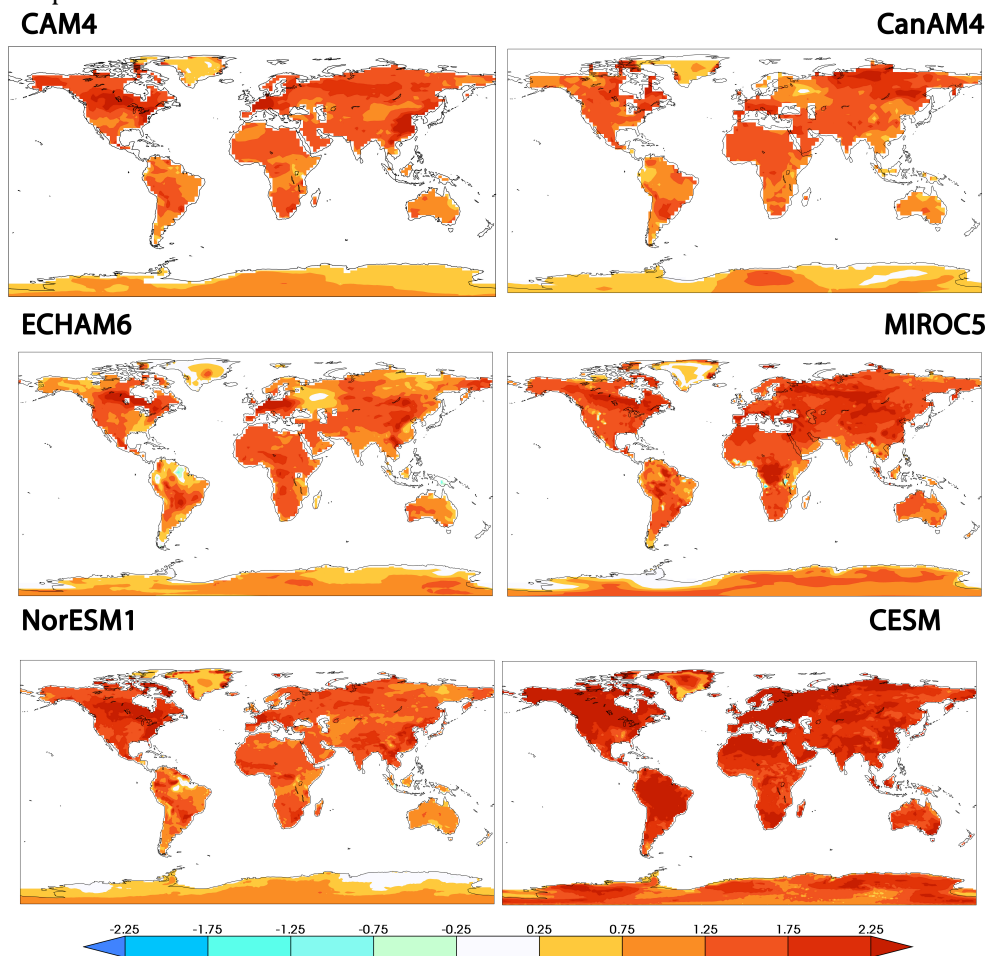


238
239 Figure 2. Differences in average hot season surface air temperature ($^{\circ}\text{C}$) between the
240 1.5 $^{\circ}\text{C}$ and present day HAPPI simulations. Upper left: CAM4. Upper right: CanAM4.
241 Middle left: ECHAM6. Middle right: MIROC5. Lower left: NorESM1. Lower right:
242 CESM.

243
244 Figure 3 shows the changes over land in 20 year return values of the annual
245 maximum of the three day average of daily maximum surface air temperatures
246 between the 2.0 $^{\circ}\text{C}$ stabilized scenario and the present day simulations. As might be
247 expected, extreme temperature increases are larger than in the 1.5 $^{\circ}\text{C}$ stabilized
248 scenario (figure 1). In this warmer scenario, most models produced no decreases in
249 extreme temperature. Only ECHAM6 has a small decrease in the Amazon. For
250 completeness, differences between the 2.0 $^{\circ}\text{C}$ stabilized scenario and the present day
251 simulations of the average surface air temperature in the hottest season are shown
252 in the Appendix. As in the cooler scenario, global averaged land extreme



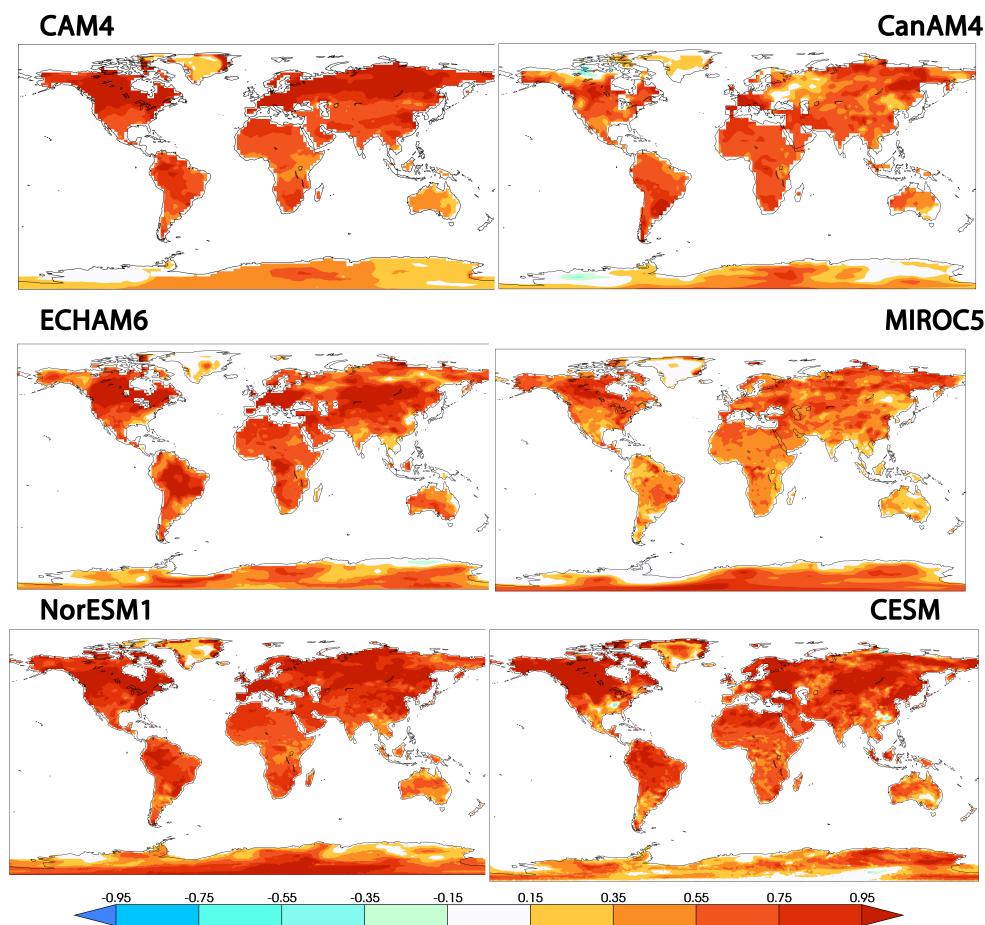
253 temperature differences are generally smaller than for the average hot season
254 temperature differences (Table 1). MIROC5, discussed in more detail below, is an
255 exception to this conclusion.



256
257 Figure 3. Change in 20 year return values ($^{\circ}\text{C}$) between the 2.0 $^{\circ}\text{C}$ and present day
258 HAPPI simulations of TX3x. Upper left: CAM4. Upper right: CanAM4. Middle left:
259 ECHAM6. Middle right: MIROC5. Lower left: NorESM1. Lower right: CESM.

260
261 Differences between the extreme temperatures of the 2.0 $^{\circ}\text{C}$ and 1.5 $^{\circ}\text{C}$ stabilized
262 scenarios are shown in figure 4. Global land average differences in extreme 3 day
263 hot temperatures range from about 0.5 $^{\circ}\text{C}$ to 0.75 $^{\circ}\text{C}$ (Table 1).

264
265

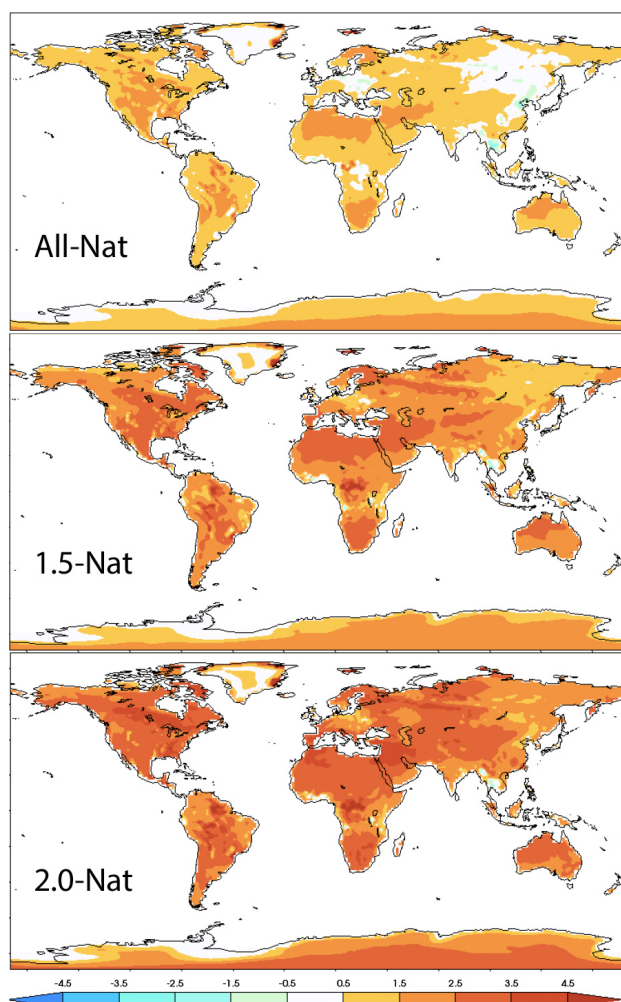


266
267 Figure 4: Differences in 20 year return values ($^{\circ}\text{C}$) between the 2.0 $^{\circ}\text{C}$ and 1.5 $^{\circ}\text{C}$
268 HAPPI simulations of TX_{3x} . Upper left: CAM4. Upper right: CanAM4. Middle left:
269 ECHAM6. Middle right: MIROC5. Lower left: NorESM1. Lower right: CESM. Note that
270 the color scale covers a smaller range of temperature differences than for the
271 previous figures.
272

273 At this time, only a single coupled model, the CESM, has been run under 1.5 $^{\circ}\text{C}$ and
274 2 $^{\circ}\text{C}$ stabilization conditions. Fortunately, a moderately sized ensemble of those
275 CESM simulations is available and analyzed in Sanderson et al. (2017) and shown in
276 the lower right panel of figures 1-4. The reference period from the “historical” run in
277 Sanderson et al. (2017) was earlier than for the HAPPI All-Hist and partly explains
278 the larger changes in the comparison between stabilization and current simulations
279 shown in figures 1-3. Although the method to simulate stabilized climates is quite
280 dissimilar between the HAPPI and the coupled model, differences between the 1.5 $^{\circ}\text{C}$



281 and 2.0°C stabilized CESM simulations of *TX3x* return values are quite similar to
282 CAM4, ECHAM6 and NorESM1 with global averages over land of 0.7°C or larger.
283
284 The MIROC5 is the only model for which results were submitted to both the C20C+
285 Detection and Attribution Project. In Wehner et al. (2017), we find that
286 anthropogenic aerosol forcing can play a critical role in heat wave attribution
287 statements. The MIROC5 experiments were run with a fully prognostic sulfate, black
288 carbon and organic carbon aerosol package forced by prescribed aerosol emissions.
289 In such experiments, aerosol concentrations can interact with the immediate
290 meteorology, leading in some regions to cooling, especially in events characterized
291 by persistent and stagnant air masses. This is indeed the case for the MIROC5 All-
292 Hist simulations compared to the C20C+ counterfactual simulations (Nat-Hist) of a
293 world without anthropogenic changes to the composition of the atmosphere. All-
294 Hist minus Nat-Hist extreme temperature from MIROC5 are replotted from Wehner
295 et al. (2017) in the top panel of figure 5 with a wider color scale to permit additional
296 comparison to the warmer stabilization scenarios. Decreases in extreme
297 temperatures are found in East Asia, the Congo and Eastern Europe that are
298 attributable to sulfate and organic carbon aerosol concentration differences for this
299 model. In the MIROC5 stabilization runs, sulfate and organic carbon aerosol
300 emissions are reduced according to the protocols of the RCP2.6 scenario. These
301 reductions allow the greenhouse gas contribution to temperature changes to
302 dominate leading to increases in these regions when comparing the stabilization
303 experiments to either the All-Hist and Nat-Hist MIROC5 experiments (figures 1,3
304 and 5). In fact, the cooling in these regions in the MIROC5 All-Hist experiment
305 results in localized hot spots when compared to the stabilization experiments
306 (figures 1 and 3). This is especially evident over the Congo in these figures.



307
308 Figure 5: Change in 20 year return values ($^{\circ}\text{C}$) of TX_{3x} between the C20C+ D&A
309 counterfactual simulation of a non-industrial world and the present day, 1.5 $^{\circ}\text{C}$, 2.0 $^{\circ}\text{C}$
310 HAPPI simulations for the MIROC5 model. Note that the color scale covers a larger
311 range of temperature differences than for the previous figures.
312

313 Conclusions.

314 The Half A degree additional warming, Prognosis and Projected Impacts (HAPPI)
315 coordinated climate modeling experiments demonstrates that there are indeed
316 benefits in the form of reduced heat wave intensities associated with lower
317 stabilization targets. The large number of realizations permits estimation of these
318 reductions in heat wave magnitude to a high precision for each of the four
319 participating models. For two of the models (CanAM4, MIROC5), heat wave
320 differences between the 1.5 $^{\circ}\text{C}$ and 2 $^{\circ}\text{C}$ stabilization targets called for in the Paris
321 Agreement are close to 0.5 $^{\circ}\text{C}$ over large portions of the land mass. The other 3



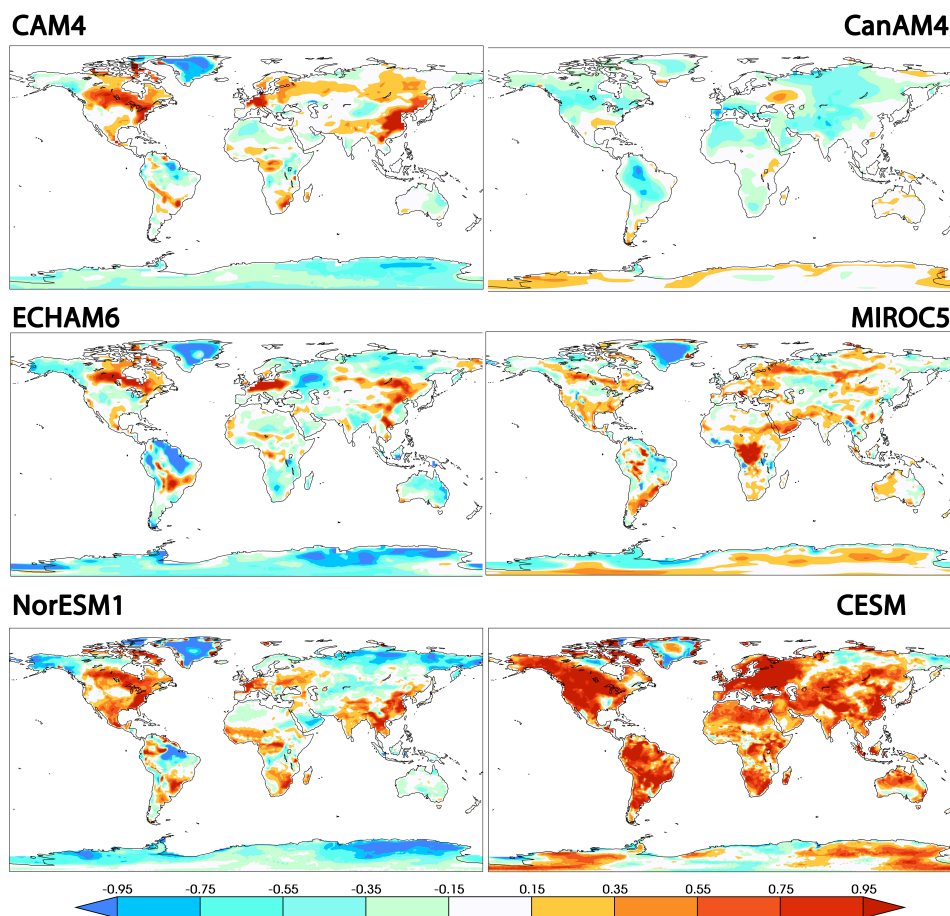
322 models showed reductions of approximately 0.75°C over large regions of the land
323 mass.

324
325 The HAPPI experimental protocol was designed to explore roughly equal
326 increments of global warming with experiments of the present day, approximately
327 1°C above preindustrial temperatures, compared to 1.5°C and 2°C above that
328 reference value. However, comparing the changes between the 1.5°C stabilization
329 and present day to the changes between the 2.0°C and 1.5°C stabilizations reveals
330 profound differences across models in the pattern of warming, both in mean and
331 extreme temperatures. This is traceable in part to the unconstrained nature of the
332 aerosol forcings. Models vary in their response to aerosol forcing, especially in the
333 so-called “indirect” effect involving feedbacks with cloud nucleation processes.
334 However, more relevant to temperature extremes are that some models prescribed
335 atmospheric aerosol concentrations while others prescribed aerosols emissions. In
336 the former case, aerosol concentrations are slowly varying and independent of the
337 local meteorology. In the latter case, aerosol concentrations interact with the
338 meteorology and can be considerably larger than their climatological averages
339 during the stagnant conditions often associated with certain types of heat waves.
340 Higher aerosol concentrations lead to greater atmospheric reflectivity reducing
341 temperatures during such heat waves. In the RCP2.6, emissions of sulfate aerosols
342 are significantly reduced compared to the present day. Hence, the type of aerosol
343 treatment can affect magnitudes of the changes in simulated *TX3x* return values.
344 Relative to the non-industrial MIROC5 simulations, present day heat waves are
345 suppressed in eastern Asia and other areas where sulfate aerosol emissions are
346 currently high. As aerosol emissions in the stabilization scenarios are reduced from
347 present day levels, changes in heat waves are larger in these regions because of this
348 suppression. This is a possible explanation of some of the differences between
349 simulated *TX3x* return values in the stabilized scenario compared to the present
350 day. On the other hand, aerosol forcing in the two stabilizations scenarios are the
351 same leading to a more controlled comparison of the effects of increased
352 greenhouse gases. As a result, the changes between stabilization scenarios in figure
353 4 are less spatially heterogeneous and more similar between models than changes
354 relative to the present day (figures 1 and 3).

355
356 This relative uniformity in figure 4 suggests that pattern scaling of extreme
357 temperature changes in models in the CMIP5 (Coupled Model Intercomparison
358 Project) forced by the RCP2.6 forcings to the 1.5°C stabilization target may be an
359 appropriate method to accurately estimate changes in extreme temperatures.
360 However, relating changes in average hot season temperatures to changes in long
361 period return values of *TX3x* is difficult in the low warming stabilization scenarios
362 considered here. Figure 6 shows the difference between changes in 20 year return
363 values of *TX3x* and hot season average temperatures for the 2.0°C stabilization
364 scenario relative to the historical period. There is no clear relationship across
365 models between changes in the middle of the temperature distribution to changes in
366 the tail. For instance, CanAM4 exhibits smaller changes in the *TX3x* return values
367 than in the hot season average. The couple model, CESM, exhibits the opposite



368 behavior. The other four HAPPI models are mixed with some regions exhibiting
369 greater changes in extreme temperatures but other regions exhibiting lesser
370 changes. The exaggerated effects on extreme temperatures of aerosol forcing
371 changes would tend to lead to larger changes in extreme temperature than for hot
372 season temperatures in the prescribed aerosol emission models since RCP2.6
373 reduces aerosol forcing. Hence, this mechanism may be partly responsible for the
374 heterogeneities in East Asia and the Congo of figure 6 but is not likely a factor for the
375 heterogeneities in North America and Europe.
376



377
378 Figure 6: Differences between changes in 20 year return values of TX_{3x} and changes
379 in hot season average temperatures ($^{\circ}C$) in the 2.0 $^{\circ}C$ HAPPI simulations. Upper left:
380 CAM4. Upper right: CanAM4. Middle left: ECHAM6. Middle right: MIROC5. Lower
381 left: NorESM1. Lower right: CESM
382



383 Land surface feedbacks offer another mechanism for different patterns of hot
384 season and extreme temperature changes. Evaporative cooling fueled by surface soil
385 moisture can locally reduce surface air temperatures (Seneviratne et al. 2010).
386 However, as the supply of surface soil moisture is limited, such temperature
387 reductions by evaporative cooling are also limited (Vogel et al 2017). Hence during
388 extended periods without rain, dry conditions can enhance extreme high
389 temperatures. If this mechanism were important, one would expect changes in
390 extreme temperatures to be larger than average hot season temperature in regions
391 with moderate amounts of hot season rainfall.

392
393 Both the aerosol forcing and land surface feedback mechanisms would lead to
394 locally larger changes in extreme temperature compared to hot season
395 temperatures. We note that both mechanisms are diminished as greenhouse gas
396 forcing increases past those imposed by the HAPPI protocols. A physical mechanism
397 for the smaller extreme temperature changes in figure 6 is not readily apparent
398 although changes in large scale circulation are certainly a possibility (Koster et al
399 2014). Also, Fischer and Schär (2009) found a lengthening of the summer season in
400 parts of Europe that could also raise the average seasonal temperature more than
401 short duration extremes. In any event, we discount the possibility that these regions
402 of smaller extreme temperature changes are a result of statistical uncertainties due
403 to the large number of HAPPI realization in each ensemble.

404
405 The lack of a clear relationship in these models between hot season and extreme
406 temperature changes apparently contradicts that found by Seneviratne et al. (2016)
407 who found an approximately linear relationship between average regional changes
408 in TXx and changes in annual global mean temperature with slopes greater than
409 unity (i.e. extremes change more than the global mean). In general, we feel that
410 comparison of changes in very hot days to hot season average temperature changes
411 is more instructive than comparison to annual mean temperature changes in order
412 to more isolate relevant physical mechanisms of changes. For instance, changes in
413 albedo due to snowmelt may cause larger winter temperature changes than
414 temperature changes in other seasons. However, the methods used to draw
415 conclusions from our study and Seneviratne et al. (2016) are too dissimilar to reveal
416 contradiction. Figure 6 shows a relationship between local temperatures for
417 individual models, while the results in Seneviratne et al. (2016) are a multi-model
418 re-expression of transient extreme temperature changes in terms of global mean
419 temperature instead of either time or greenhouse gas forcing. Such a transformation
420 of the HAPPI results would likely yield similar results.

421
422 Climate model experiments with identically prescribed sea surface temperature
423 (SST) and sea ice concentration such as presented here have a computational
424 advantage that permits large number of realizations enabling precise statistical
425 description of extreme temperatures. However, the limited number of models
426 participating in the HAPPI experiment does not sample the model structural
427 uncertainty as fully as the CMIP5 database of coupled models and the spread in
428 results presented here should not be interpreted as a complete representation of



429 the uncertainty in extreme temperature changes stabilized scenarios. Nonetheless,
430 although there is some amplification of extreme temperature differences relative to
431 average hot season temperature differences between the 1.5°C and 2.0°C
432 stabilization targets, this amplification does not appear to be dramatic.

434 **Acknowledgement**

435 This work was supported by the Regional and Global Climate Modeling Program of
436 the Office of Biological and Environmental Research in the Department of Energy
437 Office of Science under contract number DE-AC02-05CH11231. This document was
438 prepared as an account of work sponsored by the United States Government. While
439 this document is believed to contain correct information, neither the United States
440 Government nor any agency thereof, nor the Regents of the University of California,
441 nor any of their employees, makes any warranty, express or implied, or assumes any
442 legal responsibility for the accuracy, completeness, or usefulness of any information,
443 apparatus, product, or process disclosed, or represents that its use would not
444 infringe privately owned rights. Reference herein to any specific commercial
445 product, process, or service by its trade name, trademark, manufacturer, or
446 otherwise, does not necessarily constitute or imply its endorsement,
447 recommendation, or favoring by the United States Government or any agency
448 thereof, or the Regents of the University of California. The views and opinions of
449 authors expressed herein do not necessarily state or reflect those of the United
450 States Government or any agency thereof or the Regents of the University of
451 California.

452
453 Graff received support from the Norwegian Research Council, project no. 261821
454 (HappiEVA). HPC-resources for the NorESM model runs was provided in kind from
455 Bjercknes Centre for Climate Research and MET Norway. Storage for NorESM-data
456 was provided through Norstore/NIRD (ns9082k).

457
458 Shiogama was supported by the Integrated Research Program for Advancing
459 Climate Models (TOUGOU program) of the Ministry of Education, Culture, Sports,
460 Science and Technology (MEXT), Japan.

461
462 Lierhammer thanks Monika Esch, Karl-Hermann Wieners, Stefan Hagemann and
463 Thorsten Mauritsen from MPI-M for technical support with ECHAM6.3 and
464 Stephanie Legutke from DKRZ for guidance and advise. The project at DKRZ was
465 supported by funding from the Bundesministerium für Bildung und Forschung
466 (BMBF).

467



- 468 Bentsen, M., Bethke, I., Debernard, J. B., Iversen, T., Kirkevåg, A., Seland, Ø., Drange,
469 H., Roelandt, C., Seierstad, I. A., Hoose, C., Kristjánsson, J. E. Kristjánsson (2013) The
470 Norwegian Earth System Model, NorESM1-M - Part 1: Description and basic
471 evaluation of the physical climate. *Geosci. Model Dev.*, 6 (3), 687-720,
472 doi:10.5194/gmd-6-687-2013.
473
- 474 Covey, C., K. M. AchutaRao, P. J. Gleckler, T. J. Phillips, K. E. Taylor and M F. Wehner,
475 Coupled ocean-atmosphere climate simulations compared with simulations using
476 prescribed sea surface temperature: Effect of a “perfect ocean”. *Global and
477 Planetary Change* **41** (2004) 1-14
478
- 479 Fischer and Schär (2009) Future changes in daily summer temperature variability:
480 Driving processes and role for temperature extremes. *Clim. Dynam.* 33, 917–935.
481 doi:10.1007/s00382-008-0473-8
482
- 483 Gent, P. R., G. Danabasoglu, L. J. Donner, M. M. Holland, E. C. Hunke, S. R. Jayne, D. M.
484 Lawrence, R. B. Neale, P. J. Rasch, M. Vertenstein, P. H. Worley, Z.-L. Yang, and M.
485 Zhang, 2011: The Community Climate System Model Version 4. *J. Clim.*, 24 (19),
486 4973-4991, doi:10.1175/2011JCLI4083.1.
487
- 488 Hageman, S. and T. Stacke (2015) Impact of the soil hydrology scheme on simulated
489 soil moisture memory. *Clim. Dyn.*, 44, 1731-1750.
490
- 491 Hageman, S. and L. Dümenil (1997) A parameterization of the lateral waterflow for
492 the global scale. *Clim. Dyn.*, 14, 17-31.
- 493 Hosking, J. R. M., J. R. Wallis (1997) *Regional Frequency Analysis: An Approach
494 Based on L-Moments*. Cambridge University Press, 244 pages
495
- 496 IPCC, 2001: *Climate Change 2001: The Scientific Basis. Contribution of Working
497 Group I to the Third Assessment Report of the Intergovernmental Panel on Climate
498 Change. Appendix 12.3*. [Houghton, J.T., Y. Ding, D.J. Griggs, M. Noguer, P.J. van der
499 Linden, X. Dai, K. Maskell, and C.A. Johnson (eds.)]. Cambridge University Press,
500 Cambridge, United Kingdom and New York, NY, USA, 881pp
501
- 502 Iversen, T., Bentsen, M., Bethke, I., Debernard, J. B., Kirkevåg, A., Seland, Ø., Drange,
503 H., Kristjánsson, J. E., Medhaug, I., Sand, M., Seierstad, and I. A., 2013: The Norwegian
504 Earth System Model, NorESM1-M - Part 2: Climate response and scenario
505 projections. *Geosci. Model Dev.*, 6 (2), 389-415, doi:10.5194/gmd-6-389-2013.
506
- 507 Kay, J., Deser, C., Phillips, A., Mai, A., Hannay, C., Strand, G., Arblaster, J., Bates, S.,
508 Danabasoglu, G., Edwards, J., Holland, M., Kushner, P., Lamarque, J.-F., Lawrence, D.,
509 Lindsay, K., Middleton, A., Muñoz, E., Neale, R., Oleson, K., Polvani, L., Vertenstein, M.:
510 The Community Earth System Model (CESM) large ensemble project: a community
511 resource for studying climate change in the presence of internal climate variability,
512 *B. Am. Meteorol. Soc.*, 96, 1333–1349, 2015



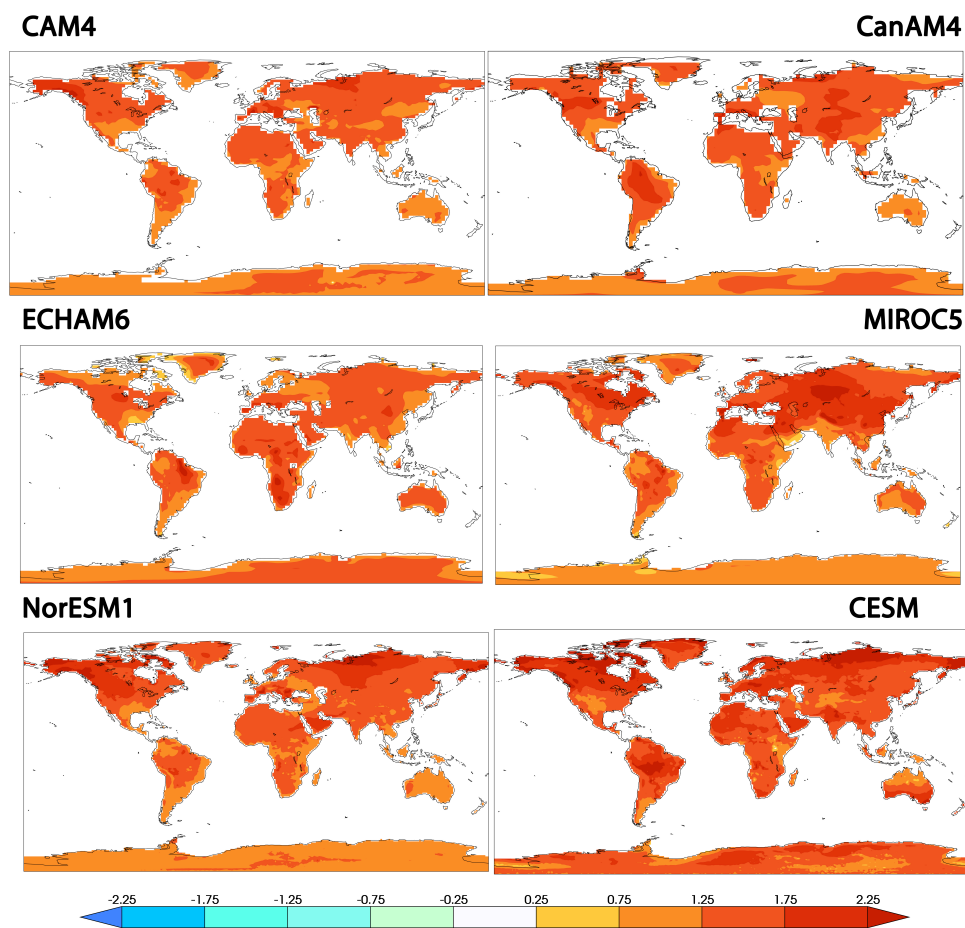
513
514 Kirkevåg, A., T. Iversen, Ø. Seland, C. Hoose, J. E. Kristjánsson, H. Struthers, A. M. L.
515 Ekman, S. Ghan, J. Griesfeller, E. D. Nilsson, and M. Schulz, 2013: Aerosol-climate
516 interactions in the Norwegian Earth System Model – NorESM1-M. *Geosci. Model*
517 *Dev.*, 6 (1), 207–244, doi:10.5194/gmd-6-207-2013.
518
519 Koster, R. D., Y. Chang, S. D. Schubert (2014), A mechanism for land-atmosphere
520 feedback involving planetary wave structures, *J. Clim.*, 27, 9290–9301.
521
522 Mitchell, D., AchutaRao, K., Allen, M., Bethke, I., Forster, P., Fuglestvedt, J., Gillett, N.,
523 Hausteiner, K., Iversen, T., Massey, N., Schleussner, C.-F., Scinocca, J., Seland, Ø.,
524 Shiogama, H., Shuckburgh, E., Sparrow, S., Stone, D., Wallom, D., Wehner, M., and
525 Zaaboul, R.: Half a degree Additional warming, Projections, Prognosis and Impacts
526 (HAPPI): Background and Experimental Design (2017). *Geosci. Model Dev.* 10, 571-
527 583, <https://doi.org/10.5194/gmd-10-571-2017>, 2017
528
529 Neale, R. B., and Coauthors, 2011: Description of the NCAR Community Atmosphere
530 Model (CAM4). NCAR Tech. Note NCAR/TN-485+STR, National Center for
531 Atmospheric Research, Boulder, CO 120 pp.
532
533 Oleson, K.W., D.M. Lawrence, G.B. Bonan, M.G. Flanner, E. Kluzek, P.J. Lawrence, S.
534 Levis, S.C. Swenson, P.E. Thornton, A. Dai, M. Decker, R. Dickinson, J. Feddema, C.L.
535 Heald, F. Hoffman, J.-F. Lamarque, N. Mahowald, G.-Y. Niu, T. Qian, J. Randerson, S.
536 Running, K. Sakaguchi, A. Slater, R. Stockli, A. Wang, Z.-L. Yang, Xi. Zeng, and Xu.
537 Zeng, 2010: Technical Description of version 4.0 of the Community Land Model
538 (CLM). NCAR Tech. Note NCAR/TN-478+STR, National Center for Atmospheric
539 Research, Boulder, CO, 257 pp.
540
541 Reick, C. H., et al. (2013) Representation of natural and anthropogenic land cover
542 change in MPI-ESM, *J. Adv. Modeling Earth Sys.* 5, 459-482.
543
544 Tebaldi C., M. Wehner (2016) Benefits of mitigation for future heat extremes under
545 RCP4.5 compared to RCP8.5. *Climatic Change*. DOI:10.1007/s10584-016-1605-5
546
547 Sanderson, B.M., Y. Xu, C. Tebaldi, M. Wehner, B. O'Neill, A. Jahn, A. G. Pendergrass, F.
548 Lehner, W. G. Strand, L. Lin, R. Knutti, and J. F. Lamarque (2017) Community Climate
549 Simulations to assess avoided impacts in 1.5 °C and 2 °C futures. *Earth Syst. Dyn.* 8,
550 827-847. <https://doi.org/10.5194/esd-8-827-2017>
551
552 Seneviratne, S.I., T. Corti, E. L. Davin, M. Hirschi, E. B. Jaeger, I. Lehner, B. Orlowsky,
553 A. J. Teuling (2010) Investigating soil moisture–climate interactions in a changing
554 climate: A review, *Earth-Science Reviews*, 99, Pages 125-161. ISSN 0012-8252,
555 <https://doi.org/10.1016/j.earscirev.2010.02.004>.
556



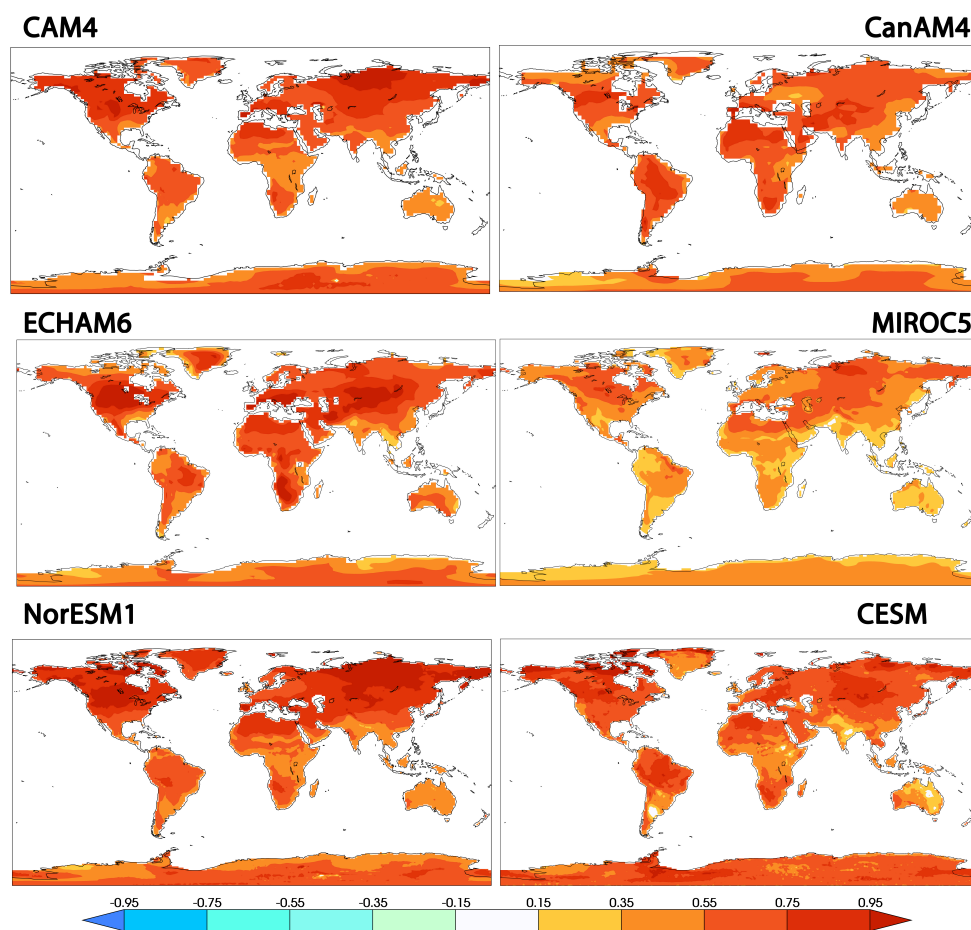
- 557 Shiogama, H., M. Watanabe, Y. Imada, Y., M. Mori, M. Ishii, M. Kimoto (2013) An
558 event attribution of the 2010 drought in the South Amazon region using the MIROC5
559 model. *Atmos. Sci. Lett.* 14, 170-175
560
- 561 Shiogama, H., M. Watanabe, Y. Imada, Y., M. Mori, Y. Kamae, M. Ishii, M. Kimoto
562 (2014) Attribution of the June-July 2013 heat wave in the southwestern United
563 States, *SOLA*, 10, 122-126, doi:10.2151/sola.2014-025
564
- 565 Sillmann, J., V. V. Kharin, X. Zhang, F. W. Zwiers, and D. Bronaugh (2013), Climate
566 extremes indices in the CMIP5 multimodel ensemble: Part 1. Model evaluation in the
567 present climate, *J. Geophys. Res. Atmos.*, 118, 1716-1733, doi:10.1002/jgrd.50203.
568
- 569 Stevens, B., et al. (2013) Atmospheric component of the MPI-M Earth System Model:
570 ECHAM6, *J. Adv. Modeling Earth Sys.*, 5, 146-172.
- 571 Tebaldi, C. & Arblaster, J.M. Pattern scaling: Its strengths and limitations, and an
572 update on the latest model simulations *Climatic Change* (2014) 122: 459.
573 <https://doi.org/10.1007/s10584-013-1032-9>
- 574 Vogel, M. M., R. Orth, F. Cheruy, S. Hagemann, R. Lorenz, B. J. J. M. van den Hurk, S. I.
575 Seneviratne (2017), Regional amplification of projected changes in extreme
576 temperatures strongly controlled by soil moisture-temperature feedbacks, *Geophys.*
577 *Res. Lett.*, 44, 1511–1519, doi:10.1002/2016GL071235.
578
- 579 von Salzen, K., J. F. Scinocca, N. A. McFarlane, J. Li, J. N. S. Cole, D. Plummer, D.
580 Verseghy, M. C. Reader, X. Ma, M. Lazare, L. Solheim (2013) The Canadian Fourth
581 Generation Atmospheric Global Climate Model (CanAM4). Part I: Representation of
582 Physical Processes. *Atmosphere-Ocean Vol.* 51, 104–125
583
- 584 Wehner, M. F., D. Stone, H. Shiogama, P. Wolski, A. Ciavarella, N. Christidis, H.
585 Krishnan (2017) Early 21st century anthropogenic changes in extremely hot days as
586 simulated by the C20C+ Detection and Attribution multi-model ensemble. Submitted
587 to *Weather and Climate Extremes* special C20C+ issue.
- 588 Zhang, X., L. Alexander, G.C. Hegerl, P. Jones, A.K. Tank, T.C. Peterson, B. Trewin, F.W.
589 Zwiers (2011), Indices for monitoring changes in extremes based on daily
590 temperature and precipitation data. *WIREs Clim Change*, 2: 851–870.
591 doi:10.1002/wcc.147
592



593 Appendix
594



595
596 Figure A1. Differences in average hot season surface air temperature (°C) between
597 the 2.0°C and present day HAPPI simulations. Upper left: CAM4. Upper right:
598 CanAM4. Middle left: ECHAM6. Middle right: MIROC5. Lower left: NorESM1. Lower
599 Right. CESM.
600
601



602
603 Figure A2: Differences in average hot season surface air temperature (°C) between
604 the 2.0°C and 1.5°C 2.0°C HAPPI simulations. Upper left: CAM4. Upper right:
605 CanAM4. Middle left: ECHAM6. Middle right: MIROC5. Lower left: NorESM1. Lower
606 Right. CESM.



Model	Resolution (#lat X #long)	Number of realizations (Nat-Hist/All-Hist /Plus15/Plus20)	Global land average change in hot season mean temperature (°C)					Global land average change in very extreme temperature (°C)				
			All- Hist Minus Nat- Hist	Plus15 minus All-Hist	Plus20 minus All-Hist	Plus20 minus Plus15	All- Hist Minus Nat- Hist	Plus15 minus All-Hist	Plus20 minus All-Hist	Plus20 minus Plus15	Plus20 minus Plus15	
CAM4	96x144	--/500/500/500	--	0.69	1.33	0.64	--	0.64	1.34	0.71		
CanAM4	64x128	--/100/100/100	--	0.80	1.40	0.60	--	0.66	1.23	0.58		
ECHAM6- 3-LR	96x192	--/100/100/100	--	0.70	1.36	0.65	--	0.48	1.12	0.69		
MIROC5	128x256	50/50/50/50	1.03	1.02	1.46	0.44	0.99	1.01	1.49	0.48		
NorESM1	192x288	--/125/125/125	--	0.72	1.41	0.70	--	0.61	1.37	0.77		
CESM1		--/40/10/10	--	0.89	1.39	0.50	--	1.45	2.2	0.74		

Table 1. Details of the HAPPI models used in this study. The number of realizations is for each part of the numerical experiment separately as used in this study. For some individual years of the All-Hist and Nat-Hist simulations, additional realizations may be available. The two rightmost columns shows the globally averaged difference between selected combinations of the hot season temperature and the 20 year return value of the annual maximum 3 day average daily



maximum surface air temperature (TX3x) over land. “Hot season” is defined as the maximum of JJA and DJF averages. Plus2.0 denotes the 2°C stabilization scenario, Plus1.5 denotes the 1.5°C stabilization scenario. Note that CESM1 is not part of the HAPPI experiment but a fully coupled ocean-atmosphere climate model that has been run with emissions scenarios consistent with both targets. The CESM1 experiments are roughly comparable to the HAPPI experiment but not exactly the same forcing or reference period.